Journal of Solid State Chemistry 183 (2010) 2979–2986

Contents lists available at ScienceDirect

Journal of Solid State Chemistry

journal homepage: www.elsevier.com/locate/jssc

Synthesis, characterization and study of arsenate adsorption from aqueous solution by α- and δ-phase manganese dioxide nanoadsorbents

Mandeep Singh [a], Dong Nguyen Thanh [b,*], Pavel Ulbrich [c], Nina Strnadová [b], František Štěpánek [a]

[a] Laboratory of Chemical Robotics, Department of Chemical Engineering, Institute of Chemical Technology, Technicka 5, 166 28 Prague 6, Czech Republic
[b] Department of Water Technology and Environmental Engineering, Institute of Chemical Technology, Technicka 5, 166 28 Prague 6, Czech Republic
[c] Department of Biochemistry and Microbiology, Institute of Chemical Technology, Technicka 5, 166 28 Prague 6, Czech Republic

ARTICLE INFO

Article history:
Received 24 May 2010
Received in revised form
10 September 2010
Accepted 19 September 2010
Available online 8 October 2010

Keywords:
Water treatment
Manganese dioxides
Nanoadsorbents
As(V) adsorption
Adsorption isotherm

ABSTRACT

Single-phase α-MnO_2 nanorods and δ-MnO_2 nano-fiber clumps were synthesized using manganese pentahydrate in an aqueous solution. These nanomaterials were characterized using the Transmission Electron Microscope (TEM), Field Emission Scanning Electron Microscope (FE-SEM), Powder X-ray diffraction (XRD) and the Brunauer–Elmet–Teller nitrogen adsorption technique (BET-N_2 adsorption). The structural analysis shows that α-MnO_2 (2×2 tunnel structure) has the form of needle-shaped nanorods and δ-MnO_2 (2D-layered structure) consists of fine needle-like fibers arranged in ball-like aggregates. Batch adsorption experiments were carried out to determine the effect of pH on adsorption kinetics and adsorption capacity for the removal of As(V) from aqueous solution onto these two types of nanoadsorbents. The adsorption capacity of As(V) was found to be highly pH dependent. The adsorption of As(V) onto α-MnO_2 reached equilibrium more rapidly with higher adsorption capacity compared to δ-MnO_2.

1. Introduction

The toxicity to humans of arsenic (As) in the environment is a major concern, shown by the World Health Organization (WHO) by recommending a limit of 10 $\mu g\,l^{-1}$ (micrograms per liter) of arsenic for drinking water that many developed nations had adopted as a regulatory standard [1]. Arsenic enters the environment through both natural and anthropogenic sources, and exists in four major oxidation states (−3, 0, +3 and +5), although the predominant forms of As in soil and water are as inorganic arsenate (As(V)) and arsenite (As(III)) [2]. Arsenate is more prevalent in oxygenated surface water while arsenite is more likely to occur in anaerobic groundwater [3,4]. Actual valence states vary from place to place depending on the redox water environment. As(III) is more toxic and difficult to remove from aqueous environment than As(V), therefore it is often being oxidized to As(V) by various techniques prior to removal. Finding out an effective technology for removing both forms of arsenic is a challenge and it depends upon various parameters like cost, secondary products that should not be harmful to the environment, availability of the materials, their storage and transportation under different environmental conditions, etc. [4].

Various treatment methods such as ion exchange [5], surface sorption [6], oxidation–precipitation [7], coagulation/electrocoagulation [8], etc. have so far been adopted for the removal of arsenic from aqueous media. Out of these, the surface sorption method by various adsorbents has the edge over other methods due to low operating and waste treatment costs, lower volume and easier-to-remove sludge formation, less consumption of reagents and their relatively easy transportation and storage [9].

With the rapid development in various characterization techniques like Transmission Electron Microscopy (TEM), Scanning Electron Microscopy (SEM) or X-ray diffractiometery (XRD) it become easier to observe the physico-chemical behavior of adsorbent materials under different conditions in the nanoscale. According to the characteristic dimensions of their principal structural features, adsorbents can be classified into two types: (a) conventional/natural/microstructured adsorbents and (b) nanostructured adsorbents. Till present, various widely used conventional microstructured adsorbents include cerium exchanged zeolites [10], clays [11], activated carbon [12], biomasses [13], etc. But in comparison to microstructured adsorbents, the nanostructured adsorbents have several advantages such as higher surface to volume ratio or smaller quantity of produced secondary pollutants. Till present nanocrystalline titanium oxide [14], nano iron (III)–zirconium (IV) bimetal mixed oxide (NHIZO) [2], nano-akaganeite [15] and other nano-structured compounds have been tested for the arsenic sorption from aqueous solutions.

Mn-oxide minerals, which occur in three polymorphic forms in nature (α-, β- and δ-MnO_2) commonly have large surface area and more passive and active sites, allowing high adsorption and excellent oxidation and catalysis activity [16,17]. Among various shapes and sizes observed in the literature the α-MnO_2

* Corresponding author.
E-mail address: Dong.Nguyen.Thanh@vscht.cz (D.N. Thanh).

0022-4596/$ - see front matter © 2010 Elsevier Inc. All rights reserved.
doi:10.1016/j.jssc.2010.09.023

nanorod structure, which is a 2×2 channeled MnO_2 phase, is very promising for the intercalation phenomenon as compared to layered birnessite [18,19]. In the present study, the nanoadsorbents of the δ-(ball like) and α-(rod like) Mn-oxide were synthesized and investigated for the removal of As(V) from aqueous solutions. According to classification, the δ-MnO_2, also known as manganous–magnetite or birnessite, is a naturally occurring, poorly crystalline 2D hexagonal layered structured oxide of tetravalent manganese, constructed of edge sharing [MnO_6] octahedra separated by a layer of water molecules and foreign ions (Na^+, K^+ and Ca^{2+}) with dendritic morphology. α-MnO_2 is a single phased octahedral molecular sieve based on a 2×2 tunnel structure composed of edge-sharing [MnO_6] octahedral with double chains [20]. The objective of this study was to synthesize and characterize the Mn-oxides nanoadsorbents and to determine their As(V) adsorption efficiencies from the aqueous medium.

2. Materials and methods

2.1. Materials and instruments

All chemicals were reagent grade and they were used without further purification. Sodium hydroxide (NaOH, 98%) was purchased from Merck, nitric acid (HNO_3) from Fisher, $MnSO_4\cdot5H_2O$ from Chemapol Praha, potassium permanganate ($KMnO_4$), hydrochloric acid (HCl) and potassium nitrate (KNO_3) from Sigma–Aldrich. A stock solution of 1000 ppm As(V) was prepared by dissolving sodium arsenate heptahydrate salt ($Na_2HAsO_4\cdot7H_2O$) from Sigma–Aldrich in distilled water. The As(V) solutions of the required concentrations for adsorption experiments were made by diluting the stock solution with 0.2% (v/v) HCl. Throughout the experiment we used double distilled water by Elga pure lab equipment (resistivity 18 MΩ cm).

For structural characterization we use TEM (JEOL JEM-1010, USA) operated at 80 kV. XRD patterns were recorded with a PANalytical X'pert PRO, Netherlands, diffractometer with Cu*K*α radiation (λ: 1.5406 Å) at room temperature operated at 40 kV. Data evaluation was performed in the software package HighScore Plus, Full Powder Pattern Analysis Software v2.2 (PANalytical, Netherlands). Surface analysis was done using FE-SEM (Hitachi S-4700 and JEOL JSM-6480LV). The average specific surface area was determined by the Brunauer–Elmet–Teller nitrogen adsorption method (BET-N_2 adsorption) along with the pore size and pore volume using the Micromeritics ASAP 2020 analyzer. pH was determined using the WTW inoLab pH-meter 720. Arsenic concentrations were determined by flameless graphite furnace atomic absorption spectrometer (Varian SpectrAAS 880). To verify the presence of arsenic and determine the oxidation state of adsorbed arsenic on the surface of Mn-oxides (MK and BR), X-ray photoelectron spectroscopy (XPS) was performed on an Omicron Nanotechnology spectrometer (GB) using a monochromatic Al Ka X-ray source (1486.7 eV) at 15 kV. The take-off angle was 80°. Mn-oxides were prepared for XPS analysis by contacting 0.5 g Mn-oxides with 50 ml solutions of As(V) at a concentration of 500 mg l^{-1} for 10 h and washing to remove unadsorbed As(V). SIGMA Laboratory (Type: 3–15, Germany) was used for centrifugation. The pH point of zero charge (pH_{PZC}) of the nanoadsorbents was determined by the solid addition method [21].

2.2. Synthesis of nanoadsorbents

2.2.1. Synthesis of α-MnO_2 nanorods

The α-MnO_2 nanorods were synthesized using manganese sulfate, $MnSO_4\cdot5H_2O$ as a precursor using a slight modification of the Mckenzie method [20] in the following way: 2.2 g of $KMnO_4$ in 40 ml in double distilled water was added to a 250 ml round bottom flask at room temperature and then heated in a 60 °C water bath for 30 min (solution A). Then 3.775 g of $MnSO_4\cdot5H_2O$ was added to 50 ml of a 2 M CH_3COOH solution and stirred at room temperature for 20 min (solution B). Solution B was then quickly poured into solution A under vigorous stirring and kept in a water bath at 80 °C for 2 h. The solution was then allowed to cool at ambient conditions to room temperature. After cooling, the resulting solution was centrifuged at 10,000 rpm. Then the particles were collected and washed several times with doubled distilled water. Finally, the samples were dried in vacuum at 50 °C and collected for further studies. Samples prepared according to the above procedure will further be denoted as MK. The general structural representation of α-MnO_2 is shown in Fig. 1(a).

2.2.2. Synthesis of birnessite (δ-MnO_2)

The birnessite particles were synthesized using manganese sulfate, $MnSO_4\cdot5H_2O$ as a precursor in the following way: 1 g of $KMnO_4$ was dissolved in 60 ml of deionised water under stirring at 600 rpm and subsequently heated on 300 °C hotplate until it starts boiling (solution A). Then 0.167 g of $MnSO_4\cdot5H_2O$ was dissolved in 20 ml of deionised water (solution B). Then solution B was poured into solution A under vigorous stirring at 600 rpm and kept at 50 °C for 1 h. The solution was then allowed to cool to room temperature at ambient conditions. After cooling, the resulting solution was centrifuged at 8000 rpm to separate the particles, which were washed five times with double distilled water. Finally, the sample was dried in vacuum at 100 °C and collected for further studies. Samples prepared in this way will further be referred to as BR. The general structural representation of birnessite is shown in Fig. 1(b). Please note that previous birnessite studies confirmed that the basic structural unit is a sheet of MnO_6 octahedra and the various interlayer cations and water molecules occupied different positions in each of the three phases [22]. Therefore, the given structural representation is a general one and not specific to the various positions of the cations and the water molecules.

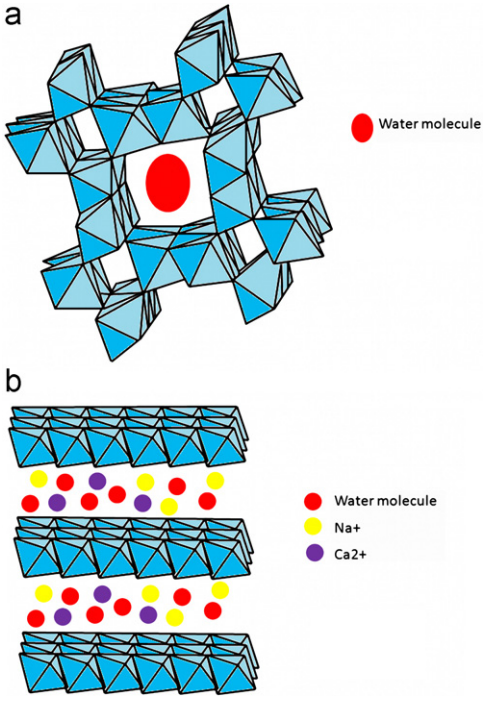

Fig. 1. General structural representation of (a) α-MnO_2 and (b) δ-MnO_2.

2.3. Batch adsorption experiment

All experiments were conducted in 250 ml Erlenmeyer flasks placed on a bench-top orbital shaker table (200 rpm) at a constant temperature (25 °C). The pH was adjusted using 0.01 N HNO_3 and 0.01 N NaOH. The effect of pH on the adsorption of arsenate was studied by mixing 0.05 g of adsorbent with 100 ml of 20 mg l^{-1} arsenate solution and varying the initial pH of the solutions between 2 and 9 for 24 h. The adsorption kinetics of arsenate on the adsorbents was studied by batch experiments with varying contact times. Solutions were in contact with the adsorbents for a period of time between 15 min and 8 h. The initial As(V) concentration was 5 mg l^{-1} and the pH was 6.5 ± 0.1. Adsorption isotherm experiments were performed by mixing 0.2 g of adsorbent with 100 ml of arsenate solution for a range of initial concentrations of arsenate from 5 to 200 mg l^{-1} at pH 6.5 ± 0.1.

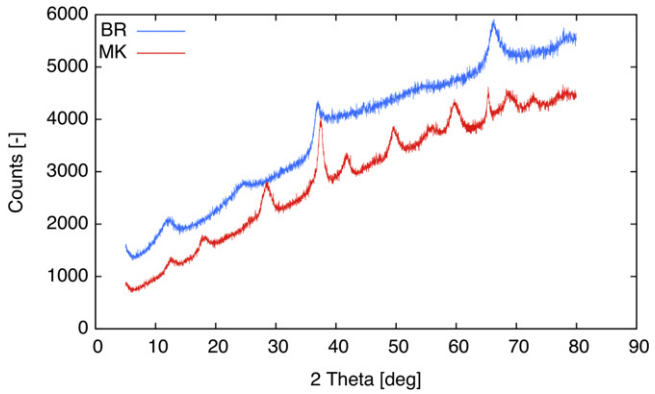

Fig. 2. X-ray diffraction patterns of the samples: α-MnO_2 and δ-MnO_2, represented as MK and BR, respectively.

The arsenic amount uptake q (mg g^{-1}) was calculated as

$$q = (C_0 - C_t)V/m \quad (1)$$

where C_0 and C_t are the concentrations of the initial and the final As(V) (mg l^{-1}), respectively, V is the volume of the solution (l) and m is the mass of adsorbent (g).

3. Results and discussion

3.1. Structural characterization of the as-synthesized nanoadsorbents

From Fig. 2, the prepared birnessite is indicated by four characteristic peaks at 11.8°, 24°, 37.2° and 66.42° corresponding to the miller indices (001), (002), ($\bar{1}$11) and (005) in the XRD pattern corresponding to sample BR. From the data evaluation using the Full Powder Pattern Analysis Software it was birnessite having the chemical formula $(Na_7Ca_3)\,Mn_7O_{14} \cdot 2.8H_2O$. Thus, the layered structure of birnessite is separated by a layer of water molecules with Na^+ and Ca^{2+} as foreign identities. The broader diffraction peak with a lower intensity reflects the nanocrystalline (nanosize) nature of the material. The TEM image in Fig. 3(a) shows the two-dimensional nanoplatelet structure of birnessite with dendritic morphology. From the SEM image in Fig. 3(b), the birnessite shows the clumps (ball like aggregates) of the two-dimensional nanoplatelet structures in the size range from 50 to 100 nm which is in good agreement with the TEM results.

From Fig. 2, the prepared α-MnO_2 (sample MK) shows typical single-crystalline phases of pure MnO_2 at 12.6°, 17.98°, 28.5°,37.4°, 41.7°, 49.7°, 55.9°, 59.9°, 65.3°, 68.9° corresponding to the miller indices (110), (200), (310), (211), (301), (411), (600), (521), (002) and (541), respectively, in the XRD pattern. From the data evaluation using the Full Powder Pattern Analysis Software it was having the chemical formula of MnO_2 and no stabilizing

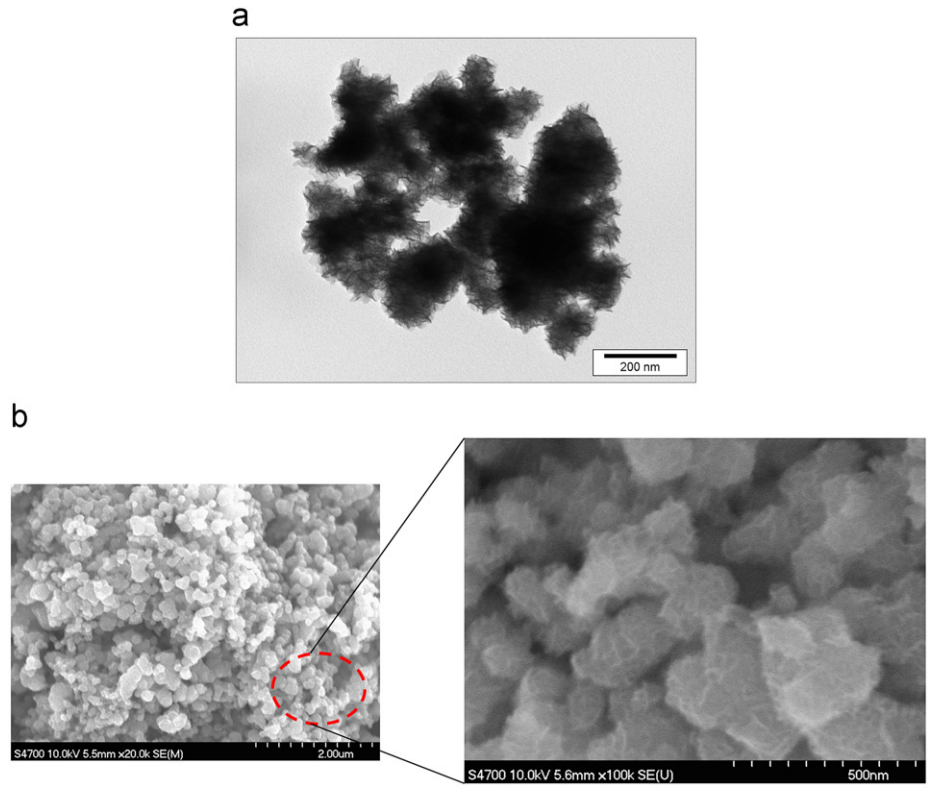

Fig. 3. (a) TEM image and (b) FE-SEM image of the as-synthesized δ-MnO_2 nanoadsorbents.

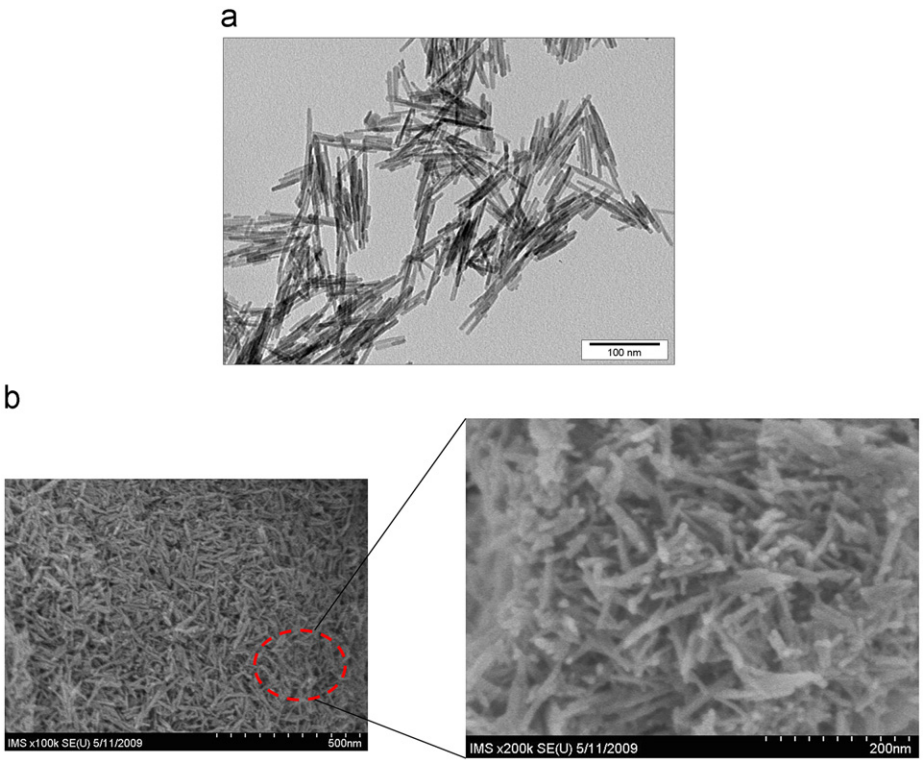

Fig. 4. (a) TEM image and (b) FE-SEM image of the as-synthesized α-MnO_2 nanoadsorbents.

cation or molecule is detected. Thus, confirming that α-MnO_2 structure is stabilized by oxygen from the water molecules within the 2×2 channels and once the powder is dry, it does not contain any water molecules attached to the tunnels. It was experimentally confirmed that oxygen ions from the water molecules residing in the (2×2) channels are close to the position normally occupied by stabilizing cations, such as K^+ in cryptomelane [23]. Compared to birnessite, the diffraction peaks in α-MnO_2 are sharper and less broadened indicating increased crystalline size, which is in good agreement with the TEM and SEM results. From the TEM in Fig. 4(a) and SEM in Fig. 4(b), the as-synthesized α-MnO_2 consists of needle shaped nanorods having a length of 50–100 nm and a width of 5 nm.

3.2. Specific surface area

The average specific surface area for the BR and MK samples along with the pore width, and pore volume are shown in Table 1. The specific surface area of MK is almost four times higher than that of BR. Further the adsorption average pore width of BR is 11.9 nm which is higher compared to MK (9.9 nm). The total pore volume of MK is 0.486 $cm^3\ g^{-1}$ which is also higher compared to the 0.166 $cm^3\ g^{-1}$ of BR.

3.3. pH point of zero charge

The pH at which the adsorbent surface has a net neutral charge is defined as the point of zero charge (pH_{PZC}). This value informs about the possible electrostatic interactions between the adsorbent and chemical species of a metal [24]. In aqueous environment, the change in the Mn-oxides nanoadsorbents surface according to the pH of the solution is as follows [25]:

$$X\text{-}OH(s)+H^+(aq)\rightarrow X\text{-}OH_2^+(s)\ (pH<pH_{PZC}) \quad (2)$$

$$X\text{-}OH(s)+OH-(aq)\rightarrow X\text{-}O-(s)+H_2O\ (pH>pH_{PZC}) \quad (3)$$

Table 1
Physical properties of α-MnO_2 (MK) and birnessite (BR).

Sample	BET surface area ($m^2\ g^{-1}$)	Average pore width (nm)	Pore volume ($cm^3\ g^{-1}$)
MK	187.3	9.9	0.486
BR	47.7	11.9	0.166

where X stands for Mn. From experimental results, the pH point of zero charge (pH_{PZC}) values calculated for MK and BR are 3.6 and 4.1, respectively.

3.4. Effect of pH on the removal of arsenate

pH is one of the most important parameters as it influences both the adsorbent surface chemistry and arsenate species in aqueous solution [25], affecting the percentage removal of arsenate. With increasing pH, the adsorbent surface increases its negative charge. In the pH range from 2 to 9, arsenate exists in the following three forms in aqueous solution: H_3AsO_4, $H_2AsO_4^-$, $HAsO_4^{2-}$ [3]. The negatively charged arsenic ion and positively charged adsorbent surface favors the arsenic adsorption. From Fig. 5(a) and (b), it is evident that the increase in pH had a negative impact on the adsorption of arsenate onto MK and BR in aqueous solution within the tested pH (2–9) range. This is attributed to the electrostatic attraction between the surface of adsorbent and the arsenate species which decrease considerably with increase in the pH value, as the presence of favorable surface sites also decreases [9,26]. A higher removal percentage below the pH_{PZC} is due to either the columbic attraction between positive surface of the adsorbent and the $H_2AsO_4^-$ or the ligand exchange phenomenon [2]. It has been reported earlier that As(V) specifically adsorbs to an oxide surface via ligand exchange

mechanisms and exists as an inner-sphere surface complex as [2,3,26,27]

$$\text{Mn-OH}+H_3AsO_4=(MnO)_2AsOOH+2H_2O$$

where Mn-OH represents a reactive hydroxyl group on the nanoadsorbents surface and $(MnO)_2AsOOH$ represents the As(V) surface complex [1]. As the pH increases, the As(V) anion changes from a monovalent ($H_2AsO_4^-$) to a divalent species ($HAsO_4^{2-}$) and there are more hydroxyl ions (OH^-) present in the solution, which increases the competition for sorption sites, thus lowering the removal percentage. Recently, it has been suggested that MnO_2 surface layers had a fixed non-renewable amount equilibrium adsorption sites for covalently bonding As(V) ions, which indicates further that As(V) adsorption is highly dependent on two factors i.e. specific surface area and pH of the aqueous medium [3,26].

3.5. Adsorption kinetics

Adsorption kinetics of the adsorbent is of great importance in the design of appropriate adsorption technologies. To describe the kinetics of the adsorption of As(V) onto Mn-oxide adsorbents, the two following models have been widely used: pseudo first-order kinetic and pseudo second-order kinetic models [28]:

$$\log(q_e-q_t)=\log q_e-(k_1/2.303)t \quad (4)$$

$$t/q_t=\left[(1/k_2q_e^2)+((1/q_e)t)\right] \quad (5)$$

where q_t and q_e are the amount of arsenate per unit weight of adsorbent (mg g^{-1}) in time (t) and at equilibrium, respectively, k_1 is the rate constant of the pseudo-first order sorption (min^{-1}) and the value was calculated from the slope of the linear plot of log (q_e–q_t) versus t. k_2 is the rate constant of the pseudo second-order adsorption and the value was calculated from the slope of the linear plot of t versus t/q_t.

Fig. 6(a) and (b) shows the kinetic data of As(V) adsorption onto MK and BR at pH=6.5. Table 2 then shows the pseudo first- and second-order model constants for As(V) adsorption on MK and BR, respectively. The calculated R^2 values for the pseudo-second order equation were 0.999 and 0.970 and those for the pseudo-first order model were 0.721 and 0.993 for MK and BR adsorbents, respectively. Thus, it can be concluded that the experimental data of adsorption kinetics of As(V) onto MK can be best described by the pseudo second-order model, while the BR adsorbent gives a slightly better fit for the pseudo first-order model. Nevertheless, let us compare the first-order kinetic rate constants in each case. The rate constant for adsorption onto MK shows higher value $k_1=0.0238$ g mg^{-1} min^{-1} compared to BR with $k_1=0.0016$ g mg^{-1} min^{-1}. The slower adsorption by BR may be attributed to the heterogeneous surface reaction or to intraparticle diffusion. As it has been reported that arsenate

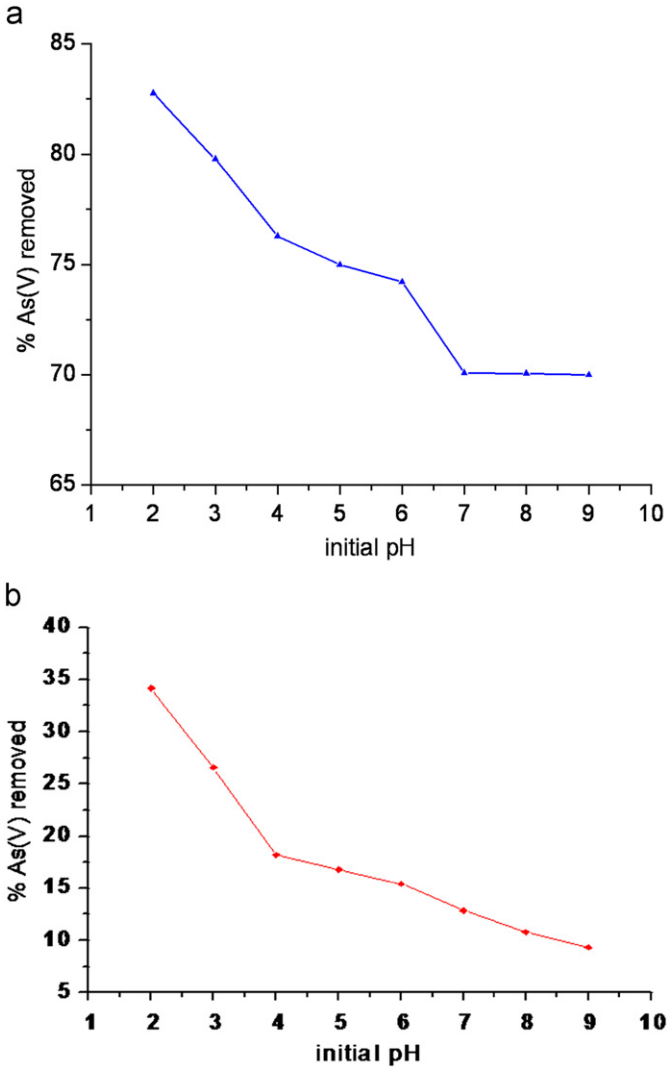

Fig. 5. Effect of pH on the removal of arsenate by Mn-oxides corresponding to (a) α-MnO_2 and (b) δ-MnO_2.

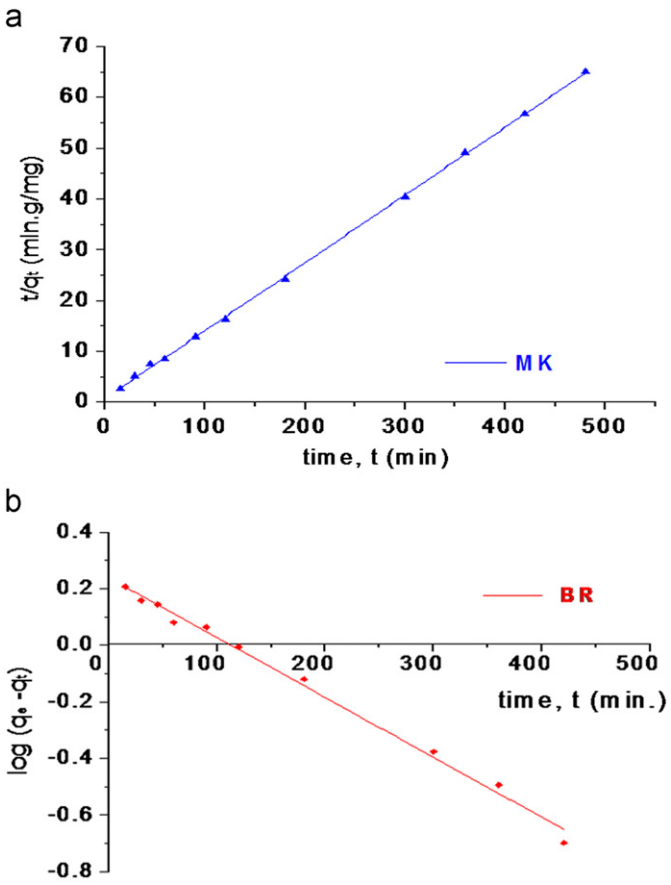

Fig. 6. (a) Pseudo-second order kinetic model plot for adsorption of arsenate onto α-MnO_2. (b) Pseudo-first order kinetic model plot for adsorption of arsenate onto δ-MnO_2 (birnessite) at pH 6.5. Both experiments are for 25 °C, the points represent experimental data and the lines are the model fits.

Table 2
Comparison of the pseudo first- and second-order adsorption rate constant.

Adsorbent	$q_{e,exp}$ (mg g^{-1})	First-order kinetics model			Second-order kinetics model		
		k_1 (min^{-1})	$q_{e,cal}$ (mg g^{-1})	R^2	k_2 (g mg^{-1} min^{-1})	$q_{e,cal}$ (mg g^{-1})	R^2
MK	7.42	0.0101	1.03	0.721	0.0238	7.50	0.999
BR	1.70	0.0048	1.73	0.993	0.0016	2.50	0.970

q_e is the amount of arsenate per unit weight of adsorbent (mg g^{-1}) in time (t) at equilibrium.
k_1 is the rate constant of pseudo-first order sorption (min^{-1}).
k_2 is the rate constant of pseudo second-order adsorption.
R^2 is the correlation coefficient values.

slow adsorption on hydrous metal oxides is most likely due to the heterogeneity of the surface site bonding energy or to the reactions occurring on the surface [29].

3.6. Adsorption isotherms

To investigate the maximum adsorption capacity of MK and BR towards As(V) and the shape of the equilibrium isotherm at pH 6.5, the adsorption isotherm data were analyzed using the linear form of the Langmuir (Eq. (6)) and the Freundlich (Eq. (7)) adsorption models as follows [30]:

$$C_e/q_e = (1/q_m K_L) + (C_e/q_m) \quad (6)$$

$$\log q_e = \log K_F + (1/n)\log C_e \quad (7)$$

where q_e (mg g^{-1}) is the adsorbed-phase equilibrium concentration, C_e (mg l^{-1}) is the liquid-phase equilibrium concentration, q_m (mg g^{-1}) is the monolayer sorption capacity, K_F and K_L are the Freundlich and Langmuir adsorption coefficients, respectively, and n is the Freundlich exponent. The plot of the linear adsorption isotherms for the Langmuir and Freundlich models are shown in Fig. 7(a) and (b) for MK and BR, respectively. The adsorption isotherm data of Langmuir and Freundlich equations were calculated and are shown in Table 3. On the basis of the linear regression coefficient (R^2) values, it could be said that the adsorption equilibrium data are better described by the Langmuir isotherm in the case of MK. On the other hand, the adsorption equilibrium data of As(V) on BR fit both the Langmuir and Freundlich isotherms fairly well, although the Freundlich isotherm is found to give a marginally better correlation coefficient. In general, the increase Freundlich (K_F) and Langmuir (K_L) adsorption coefficients values for MK as compared to BR indicate an increased in the adsorption capacity of arsenate in the aqueous solution onto their surface [33]. The adsorption capacity, q_m (mg g^{-1}) of arsenate onto MK and BR is 19.41 and 15.33 mg g^{-1}, respectively. The higher adsorption capacity of MK compared to BR puts into evidence that, even though their pH_{PZC} is quite comparable, the specific surface area, pore volume and average pore width also play a role in the adsorption of arsenate onto their surface. Additionally, XPS study was done to analyze the binding of As(V) onto the surface of MK and BR nanoadsorbents.

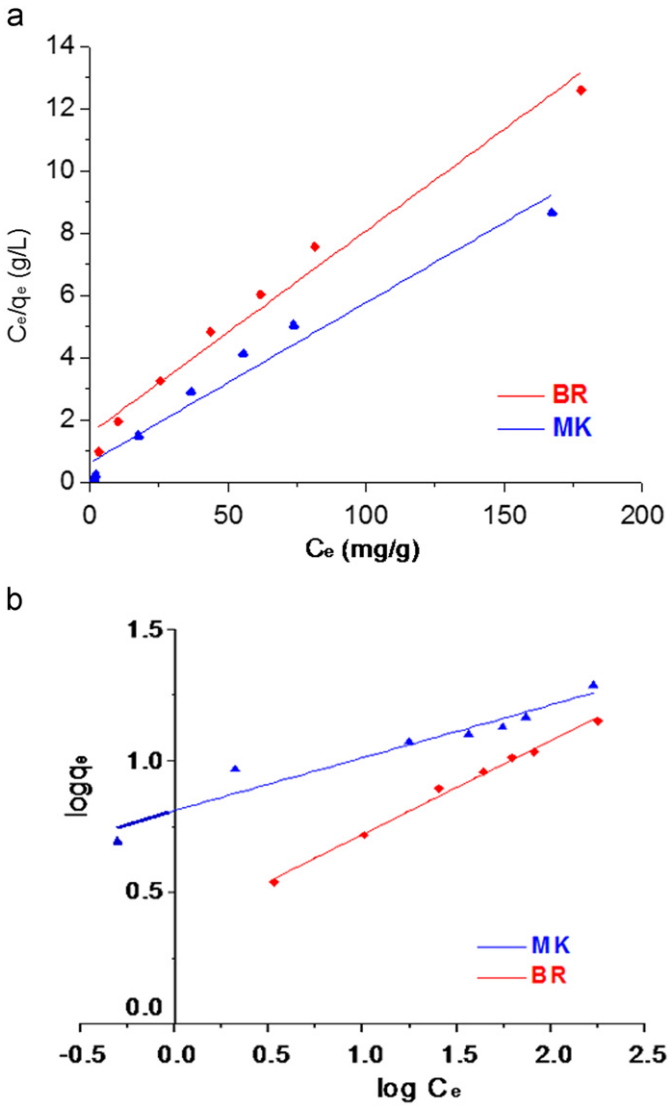

Fig. 7. Adsorption isotherms of arsenate onto Mn-oxides in a linear form (a) Langmuir model and (b) Freundlich model corresponds to α-MnO_2 (MK) and birnessite (BR), respectively, at pH 6.5 and 25 °C. The triangles represent experimental data and the lines are the model fits.

3.7. Analysis of XPS spectra

The surface of both types of nanoadsorbents was examined using XPS to verify the presence of arsenic and to determine the oxidation state of the adsorbed arsenic. As seen in Fig. 8, the As3*d* peak confirms the presence of arsenic on the surface of Mn-oxide adsorbents contacted with arsenic solution. The As3*d* peak indicates that arsenic on the surface of MK and BR is in the stable form of As(V). The peak of As3*d* is intense with the binding energy centered on 45.6 eV in case of MK, as compared to 44.8 eV for BR. Although there is no literature on the binding energies of arsenate species on MK, the As3*d* peak of As(V) on synthetic birnessite has been reported at a binding energy of 45.15 eV [3] which is near to our results. The percentage of arsenate on the surface of MK is 0.099% as compared to 0.021% on BR, clearly indicating the higher adsorption of As(V) in case of MK as

Table 3
Coefficients of determination for the fit of As(V) adsorption data onto two types of Mn-oxides at pH 6.5.

Adsorbent	Langmuir constants			Freundlich constants		
	q_m (mg g^{-1})	K_L (l mg^{-1})	R^2	n	K_F (mg g^{-1}) (l mg^{-1})$^{-1/n}$	R^2
MK	19.41	0.083	0.965	4.975	6.449	0.930
BR	15.33	0.042	0.979	2.802	2.306	0.994

q_m is the maximum adsorption capacity from the Langmuir isotherms.
K_F is a Freundlich constant related to adsorption capacity.
K_L is a Langmuir constant.
n is a dimensionless Freundlich exponent.

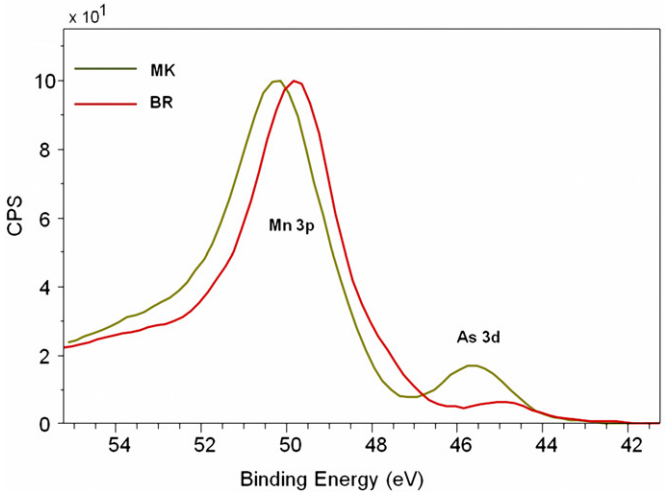

Fig. 8. XPS pattern of (a) α-MnO_2 (green color) and (b) δ-MnO_2 (red color) (for interpretation of the references to color in this figure legend, the reader is referred to the web version of this article).

Table 4
Comparison of uptake capacity for As(V) with various nanoadsorbents.

Nanoadsorbent	Initial pH	Initial concentration (mg l^{-1})	Maximum removal capacity (mg g^{-1})	References
Manganese-substituted Fe (III) oxyhydroxide	7.0	1–50	5.72	[31]
Nanoparticles CuO	8	0.1–100	22.6	[32]
Nanohydrous iron–titanium mixed mode	7	5–150	14.3	[33]
Pure titanium dioxide (nanoparticle)	7.6	5–90	20.53	[34]
Maghemite nanopowder (Sigma-Aldrich)	7.0	1–11	5.0	[9]
Crystalline hydrous ferric oxide	3–4	50–250	25	[35]
Nanostructure iron(III)–zirconium(IV) bimetal mixed oxide (NHIZO)	7	5–150	9.36	[2]
α-MnO_2 (MK)	6.5	5–200	19.41	Present work
δ-MnO_2 (birnessite, BR)	6.5	5–200	15.33	Present work

compared to BR and in agreement with the adsorption studies results.

Finally, to estimate the As(V) removal efficiency of MK and BR, the adsorption capacity (q_m) values have been compared with some reported data for different nanoadsorbents, shown in Table 4. As the q_m value of the adsorbent varies with the initial concentration range of the solute, pH, and other experimental conditions, it becomes difficult to compare directly. However, in general from the table we can conclude that MK and BR materials prepared in this work are relatively good adsorbent materials for As(V) removal from aqueous media at normal pH conditions.

4. Conclusion

In summary, Mn-oxide based nanoadsorbents are potential candidates for the adsorption of As(V). Both α- and δ-phase of MnO_2 have a high adsorption capacity for arsenate in aqueous solution. Electrostatic force and the ligand exchange (ligand exchange with –OH) phenomenon are the two factors that play an important role in the adsorption of arsenate species onto Mn-oxides surface. However, the physical properties of the Mn-oxides nanoadsorbents play a greater role. It has been observed that tunnel structured MnO_2 with high specific surface area and pore volume is more effective in the removal of As(V) from the aqueous solution than MnO_2 with a layered structure, having less specific surface area and lower pore volume. Future research could focus on the synthesis of composite adsorbents based on these nanoadsorbents and study the dynamic adsorption of As(V) in column experiments.

Acknowledgments

F.S. and M.S. are grateful for financial support by the European Research Council, project 200580-CHOBOTIX. One of the authors, Dong is thankful to Ministry of Education, Youth and Sports Czech Republic for providing Scholarship—B588/2006-61-230. Authors are also thankful to Dr. Hong Vu, Ing. J. Vítková from ICT, Prague and Dr. Tran Hong Con from VNU, Vietnam.

References

[1] WHO, Guidelines For Drinking Water Quality, 2006.
[2] K. Gupta, T. Basu, U.C. Ghosh, J. Chem. Eng. Data 54 (2009) 2222–2228.
[3] B.A. Manning, S.E. Fendorf, B. Bostick, D.L. Suarez, Environ. Sci. Technol. (2002) 976–981.
[4] S.K. Maji, A. Pal, T. Pal, J. Hazard. Mater. 151 (2008) 811–820.
[5] J. Kim, M.M. Benjamin, Water Res. 38 (2004) 2053–2062.
[6] J. Pattanayak, K. Mondal, S. Mathew, S.B. Lalvani, Carbon 38 (2000) 589–596.
[7] T. Nishimura, Y. Umetsu, Hydrometallurgy 62 (2001) 83–92.
[8] T. Yuan, Q.-F. Luo, J.-Y. Hu, S.-L. Ong, W.-J. Ng, J. Environ. Sci. Health Part A 38 (2003) 1731–1744.
[9] T. Tuutijärvi, J. Lu, M. Sillanpää, G. Chen, J. Hazard. Mater. 166 (2009) 1415–1420.
[10] M.J. Haron, F. Ab Rahim, A.H. Abdullah, M.Z. Hussein, A. Kassim, Mater. Sci. Eng. B 149 (2008) 204–208.
[11] A.H. Malik, Z.M. Khan, Q. Mahmood, S. Nasreen, Z.A. Bhatti, J. Hazard. Mater. 168 (2009) 1–12.
[12] L. Lorenzen, J.S.J. van Deventer, W.M. Landi, Miner. Eng. 8 (1995) 557–569.

[13] G.S. Murugesan, M. Sathishkumar, K. Swaminathan, Bioresource Technol. 97 (2006) 483–487.
[14] H.Y. Niu, J.M. Wang, Y.L. Shi, Y.Q. Cai, F.S. Wei, Microporous Mesoporous Mater. 122 (2009) 28–35.
[15] E.A. Deliyanni, D.N. Bakoyannakis, A.I. Zouboulis, K.A. Matis, Chemosphere 50 (2003) 155–163.
[16] D.W. Oscarson, P.M. Huang, W.K. Liaw, U.T. Hammer, Soil Sci. Soc. Am. J. 47 (1983) 644–648.
[17] X.H. Feng, L.M. Zhai, W.F. Tan, F. Liu, J.Z. He, Environ. Pollut. 147 (2007) 366–373.
[18] V.G. Kumar, K.B. Kim, Ultrason. Sonochem. 13 (2006) 549–556.
[19] I.I. Naumov, L. Bellaiche, H. Fu, Nature 432 (7018) (2004) 737–740.
[20] R.M. McKenzie, Mineral. Mag. 38 (1971) 493–502.
[21] S.S. Tripathy, S.B. Kanungo, J. Colloid Interface Sci. 284 (2005) 30–38.
[22] J.E. Post, in: Proceedings of the National Academy of Sciences of the United States of America, vol. 96, 1999, pp. 3447–3454.
[23] C.S. Johnson, D.W. Dees, M.F. Mansuetto, M.M. Thackeray, D.R. Vissers, D. Argyriou, C.K. Loong, L. Christensen, J. Power Sources 68 (1997) 570–577.
[24] N. Fiol, I. Villaescusa, Environ. Chem. Lett. 7 (2009) 79–84.
[25] P. Mondal, C. Balomajumder, B. Mohanty, J. Hazard. Mater. 144 (2007) 420–426.
[26] T. Radu, A. Kumar, T.P. Clement, G. Jeppu, M.O. Barnett, J. Contam. Hydrol. 95 (2008) 30–41.
[27] Y. Arai, E.J. Elzinga, D.L. Sparks, J. Colloid Interface Sci. 235 (2001) 80–88.
[28] K.C. Bhainsa, S.F. D'Souza, Bioresource Technol. 99 (2008) 3829–3835.
[29] J. Zhang, R. Stanforth, Langmuir 21 (2005) 2895–2901.
[30] E. Unuabonah, K. Adebowale, B. Olu-Owolabi, L. Yang, Adsorption 14 (2008) 791–803.
[31] P. Lakshmipathiraj, B.R.V. Narasimhan, S. Prabhakar, G. Bhaskar Raju, J. Colloid Interface Sci. 304 (2006) 317–322.
[32] C.A. Martinson, K.J. Reddy, J. Colloid Interface Sci. 336 (2009) 406–411.
[33] K. Gupta, U.C. Ghosh, J. Hazard. Mater. 161 (2009) 884–892.
[34] D. Nabi, I. Aslam, I.A. Qazi, J. Environ. Sci. 21 (2009) 402–408.
[35] B.R. Manna, S. Dey, S. Debnath, U.C. Ghosh, Water Qual. Res. J. Can. 38 (2003) 193–210.